0 0 0 0 4 2 0 1 1 3 3

Submitted to Journal of
Chemical Physics

LBL-3157
Preprint c.1

THE A + B_x CONDENSATION REACTION: CROSSED NOZZLE BEAMS OF Br_2 AND $(Cl_2)_x$ OR $(NH_3)_x$ CLUSTERS

Richard Behrens, Jr., Andrew Freedman,
Ronald R. Herm and Timothy P. Parr

September 1975

Prepared for the U. S. Energy Research and
Development Administration under Contract W-7405-ENG-48

For Reference

Not to be taken from this room

LAWRENCE BERKELEY LABORATORY
UNIVERSITY OF CALIFORNIA
BERKELEY

LBL-3157
c.1

DISCLAIMER

This document was prepared as an account of work sponsored by the United States Government. While this document is believed to contain correct information, neither the United States Government nor any agency thereof, nor the Regents of the University of California, nor any of their employees, makes any warranty, express or implied, or assumes any legal responsibility for the accuracy, completeness, or usefulness of any information, apparatus, product, or process disclosed, or represents that its use would not infringe privately owned rights. Reference herein to any specific commercial product, process, or service by its trade name, trademark, manufacturer, or otherwise, does not necessarily constitute or imply its endorsement, recommendation, or favoring by the United States Government or any agency thereof, or the Regents of the University of California. The views and opinions of authors expressed herein do not necessarily state or reflect those of the United States Government or any agency thereof or the Regents of the University of California.

0 0 0 0 4 2 0 1 1 3 4

LBL-3157

THE $A + B_x$ CONDENSATION REACTION: CROSSED NOZZLE BEAMS OF Br_2 AND $(Cl_2)_x$ OR $(NH_3)_x$ CLUSTERS

Richard Behrens, Jr., Andrew Freedman, Ronald R. Herm
and Timothy P. Parr

Inorganic Materials Research Division, Lawrence Berkeley Laboratory
and Department of Chemistry, University of California, Berkeley
and
Ames Laboratory - ERDA and Department of Chemistry
Iowa State University, Ames, Iowa 50010*

ABSTRACT

Nozzle beams of Br_2 and Cl_2 or NH_3 have been crossed in a molecular beam scattering apparatus; the Cl_2 or NH_3 beam contained $(Cl_2)_x$ or $(NH_3)_x$ clusters distributed such that the intensity of a given cluster, F_x, decreased with increasing x for $1 \leq x \leq \sim 50$. Mass, angular, and time-of-flight spectra of the scattered neutral species all establish that the $A + B_x \rightarrow AB_x^*$ bimolecular condensation reaction is being observed. However, the data are unable to

*Present address.

distinguish between detection of a long-lived AB_x^* metastable complex or of a decomposition product formed with low recoil velocity. Product angular distributions are confined to a small region of laboratory scattering angle Θ and peak at small but positive Θ(Θ = 0° and 90° defined by cluster and Br_2 beam directions, respectively). It is pointed out that this sharp peaking at small Θ is due to a number of experimental factors, including a Jacobian factor varying as $\sin^{-2}\Theta$, and should be a universal characteristic of such condensation reactions in crossed beams. The data indicate a high probability of fragmentation into small daughter ions upon electron bombardment (EB) ionization of an AB_x or B_x cluster for the range in x most sensitive to the measurements ($\sim 10 \leq x \leq \sim 50$). This in turn implies that the concentration of neutral clusters in the beam can be seriously underestimated if the cluster ion mass spectra produced by EB ionization of the nozzle beam are assigned assuming that fragmentation is inconsequential.

Formation of dimers and larger clusters of neutral species bound by weak electrostatic or dispersion forces is now well established in isentropic nozzle-beam expansions. The phenomenon was apparently first carefully documented by Leckenby and co-workers[1] and by Milne and Green[2]. Hagena and Obert[3] deduced scaling laws and reduced variables useful in correlating the extent of condensation in expansions from stagnation chambers of differing source pressure, P_o, temperature, T_o, nozzle diameter, d, and even gaseous species.

A variety of scattering studies employing these clusters have recently appeared. Examples include electron diffraction from Ar_x[4], electron bombardment (EB) ionization of $(H_2)_x$[5], and scattering of He_x, $(H_2)_x$, and $(N_2)_x$ from a surface[6]. The ability to generate intense cluster beams potentially extends the chemical domain of crossed beams studies of bimolecular collision dynamics to include such diverse topics as reactions pertinent to termolecular kinetics[7], gas-surface scattering as a function of surface size, and condensation of a probe particle on a large cluster. Two recent crossed beam scattering studies have exploited this condensation phenomenon. King, Dixon, and Herschbach[7] reported center-of-mass (CM) maps derived from their measured laboratory (LAB) angular and time-of-flight (TOF) distributions for reactive scattering in

$$(Cl_2)_2 + Br_2 \rightarrow Cl_2 + 2BrCl \qquad (R1)$$

and

$$(Cl_2)_2 + HI \rightarrow Cl_2 + ICl + HCl. \qquad (R2)$$

Urena, Bernstein, and Phillips [8] reported observation of K and Rb condensation on $(CH_3I)_x$, i. e.

$$M + (CH_3I)_x \rightarrow M \cdot (CH_3I)_x^* \qquad (R3)$$

where $x \gtrsim 4$ and the asterick denotes a long-lived metastable complex potentially capable of decomposition into a number of product channels.

This paper reports crossed beams studies of other condensation reactions. An uncondensed Br_2 nozzle beam has been crossed by a Cl_2 or NH_3 nozzle beam which contained substantial concentrations of heavier clusters. Figure 1 shows an angular distribution of neutral scattered species from $Br_2 + (Cl_2)_x$ measured for an m/e mass filter setting corresponding to $BrCl^+$. By convention, the LAB scattering angle, Θ, is measured from the $(Cl_2)_x$ or $(NH_3)_x$ beam with $\Theta = 90°$ taken as the Br_2 beam direction. This angular distribution is very unusual because almost all of the scattering is confined to a small range of positive Θ values near $\Theta = 0°$. The remainder of this paper reports additional mass, angular, and TOF spectra of the scattered signals which all point to a condensation of the Br_2 probe particle (chosen because of favorable kinematics by virtue of its heavy mass) on the $(Cl_2)_x$ or $(NH_3)_x$ clusters, i. e.

$$Br_2 + (Cl_2)_x \rightarrow Br_2 \cdot (Cl_2)_x^* \qquad (R4)$$

and $$Br_2 + (NH_3)_x \rightarrow Br_2 \cdot (NH_3)_x^* . \qquad (R5)$$

In referring to reactions (R3), (R4), or (R5) as "condensations" throughout the paper, however, it should be noted that the data are unable to distinguish between actual detection of a long-lived metastable complex and one of its decomposition products formed with a low recoil velocity.

EXPERIMENTAL

The apparatus has been described previously.[9] Each nozzle beam is formed by expansion through a 0.010 cm diameter hole (0.0125 cm and 0.0025 cm[10] throat thicknesses for beams 1 and 2, respectively) from a stainless steel stagnation chamber housed in a separate source vacuum chamber pumped by a 10 in oil (DC-704) diffusion pump ($\sim 2 \times 10^{-4}$ torr). The nozzle beam leaves this chamber through a skimmer, traverses an intermediate collimation vacuum chamber ($<10^{-5}$ torr), and finally enters the main vacuum chamber ($<10^{-6}$ torr) where it is intersected at 90° by the other nozzle beam. Skimmer design and measured beam conditions during various experiments are given in Table I; beam angular widths (FWHM) were 1.1° (beam 1) and 1.5° (beam 2) in Exps. II-V. Extensive cryogenic cooling is employed in the main chamber, but none is employed in either collimation chamber or source chamber.

The detector, consisting of a Brink type EB ionizer and EAI Quad-250 mass filter, is housed in a nest of three differentially pumped ultra-high vacuum chambers ($\sim 10^{-9}$ - 10^{-10} torr) which may be rotated about the beam intersection region (BIR). The electron bombardment energy was

nominally set at 110 eV throughout these experiments; actual electron energies are likely to be lower and broadly distributed, however, since the ionizer is operated near the space charge limit. Since the ionization efficiency is low even for heavy clusters, the detector signal is proportional to the number density of the neutral species being ionized. Neutral species scattered from the BIR reach the ionizer by traversing two square orifices: 0.38 cm wide, 4.4 cm from BIR and 0.30 cm wide, 18.4 cm from the BIR. This first square orifice is replaced by an 0.0075 cm diameter hole when measuring mass, angular, or TOF profiles of either nozzle beam. A fast pulsing wheel is placed immediately in front of this first detector opening when measuring the distribution in flight times (TOF spectra) of the neutral specials to the ionizer (17.4 to 21.4 cm flight path). The scattered signal is calculated as

$$\text{Signal} = N(1, 2) - N(0, 2) - [N(1, 0) - N(0, 0)] \qquad (1)$$

where N(1, 2) refers to both beams on, N(0, 2) to beam 1 off, N(1, 0) to beam 2 off, and N(0, 0) to both beams off. Beam 1 was turned on and off at 55 Hz by means of a rotating chopping wheel; a beam flag served to turn beam 2 on or off. Unless otherwise noted, all angular distribution data points were collected by counting for 120 seconds, i.e. 30 seconds for each entry in Eq. (1). Counting times varied in TOF measurements. Error bars, shown only if they are larger than a data point symbol, were calculated as $\pm [N(1, 2) + N(0, 2) + N(1, 0) + N(0, 0)]^{1/2}$.

No evidence for dimers or heavier clusters in the Br_2 beam was observed. However, clusters were easily discernible in the Cl_2 or NH_3 beam which employed higher pressure and lower temperature in the nozzle stagnation chamber. Figure 2 shows, for example, a mass spectrum of the Cl_2 beam with resolved peaks extending up to Cl_{15}^+; similar data on the NH_3 nozzle (Exp. V) showed the presence of $(NH_3)_x$ up to at least x = 6. The distribution of Cl_n^+ signals obtained in the mass spectrum of the Cl_2 nozzle of Exp. III is shown in Fig. 3. The intensity alternation for even and odd values of n in Figs. 2 and 3 is interesting. The anomalously high n = 12 peak in Fig. 3 appears to be experimental error since the effect isn't apparent in Fig. 2. In the absence of any other type of data, measurements such as those shown in Figs. 2 and 3 might be interpreted as the distribution in cluster sizes in the nozzle beam despite a number of poorly understood experimental parameters. The resolution and transmission of the quadrupole mass filter is not well understood. Data were collected at an approximately constant $\Delta m/m$ setting which should produce a transmission which is independent of or increases slowly with increasing mass. For the relatavely small cluster sizes of interest here ($x < 50$-100), recent measurements[5] indicate that the EB ionization cross section, $Q_i[(Cl_2)_x]$, should be proportional to x, a relation consistent with the well-known[11] approximate linear dependence of EB ionization cross section on molecular polarizability. Very little is known, however, about the very important question of the fragmentation pattern of the parent ion. In the past[2],

fragmentation has often been assumed to be negligible. Although this is likely to be a good approximation for the very small clusters, data presented later indicate extensive fragmentation of the larger clusters observed here.

Figure 4 presents TOF spectra of the Cl_2 nozzle of Exp. III measured at various Cl_n^+ mass filter signals. These clearly indicate that Cl_2 monomers are moving faster than are heavier species in the beam. There is also an indication of a slight shift to longer flight times and slower speeds with increasing n. Throughout this paper, measured TOF spectra are fit to corresponding number density speed distributions by convoluting over the pulsing wheel gate function and the finite ionizer length. Most of the breadth of the curves of Fig. 4 are due to this finite apparatus time resolution. These curves are well-fit by nozzle number density speed distributions of the form

$$\rho(v) = K\, v^2\, \alpha^{-3}\, \exp[-(v-u)^2/\alpha^2] \qquad (2)$$

where K, α, and u are adjustable parameters. In interpreting measured TOF spectra of scattered signals in a later section, the $(Cl_2)_x$ clusters in the beam are all assigned the same speed distribution which is arrived at by fitting Eq. (2) to the TOF spectrum of the heaviest ion signal measured in the nozzle beam; these speed distribution parameters are listed in Table I. The TOF spectra of the Br_2 beam and of the Cl_2^+ mass filter signal in the $(Cl_2)_x$ beam were always well-fit by standard

nozzle theory wherein the flow, u, and breadth, α, speed parameters are coupled through the Mach number M,

$$\alpha^2 = \alpha_o^2[1 + (C_P - C_V)M^2/2C_V]^{-1} \tag{3}$$

$$u = 0.71\ \alpha M[C_P/C_V]^{1/2}$$

where $\alpha_o = 2kT_o/m$ and C_V is calculated assuming translational and rotational relaxation in the expansion process. The fit of the Cl_2^+ TOF spectrum to Eq. (3) suggests that the beam is not strongly condensed since there is no measurable heat of condensation contribution to the flow speed, u.

RESULTS AND ANALYSIS

Mass, angular, and TOF spectra of the scattered signal all point to observation of the general condensation reaction:

$$A + B_x \rightarrow AB_x^* . \tag{R6}$$

Mass Spectra of Scattered Signal

Mass scans of the scattered signals were collected first in order to insure that the massfilter settings employed corresponded to product signals from reaction (R6) rather than elastic or inelastic scattering of B_x species in the beam. Figure 2 illustrates that this procedure consisted of insuring that: (1) the massfilter was tuned to a mass peak

in the scattered signal; and (2) this mass setting coincided with a valley in the mass spectrum of the B_x beam. In the $Br_2 + (Cl_2)_x$ experiments, mass peaks in the scattered signal have been observed at m/e mass filter settings corresponding to $BrCl^+$, $Br_2Cl_2^+$, $Br_2Cl_4^+$, $Br_2Cl_6^+$, $Br_2Cl_8^+$, and $Br_2Cl_{10}^+$. Other mass peaks (e.g., $BrCl_2^+$, Br_2Cl^+, Cl_3^+, Cl_4^+, etc.) were not examined and were probably present as well. Similarly, mass peaks at $BrNH_3^+$, $Br_2(NH_3)_2^+$, $Br_2(NH_3)_3^+$, and $Br_2(NH_3)_5^+$ were studied in the scattering of Br_2 from $(NH_3)_x$. This abundance of mass peaks in the scattered signal provided the first indication of the occurence of reactions (R4) and (R5).

Angular Distributions of Scattered Signals

Scattered angular distributions measured at the $BrCl^+$ massfilter setting for two different Cl_2 stagnation pressures (Exp. II) are shown in Fig. 5. Figures 1 and 5 indicate that the quantitative shape of the $BrCl^+$ angular distribution is dependent on the Cl_2 stagnation pressure, peaking more sharply near $\Theta = 0°$ with increasing P_o. Nevertheless, it is striking that, at all three Cl_2 stagnation pressures, the $BrCl^+$ angular distribution is confined to a small region of positive Θ near the $(Cl_2)_x$ beam. In this regard, a possible second peak in the $BrCl^+$ angular distribution in the $P_o(Cl_2) = 450$ torr experiment was sought by counting for 1200 seconds at $\Theta = 86°$ (4° from Br_2 beam). This resulted in a $BrCl^+$ signal count of 3500 ± 2000, i.e., much weaker than that at Θ=4° if present at all. In view of this qualitative invariance of the $BrCl^+$ angular distribution to P_o, all further experiments (III-V) were run at fixed nozzle stagnation pressures.

Figures 6-8 illustrate that the shape of the scattered angular distribution is approximately independent of the mass filter setting. This same effect was also observed in Exp. II (although at poorer signal to noise) where $BrCl_6^+$ and $BrCl^+$ at $P_o(Cl_2) = 450$ torr and $BrCl_8^+$ and $BrCl^+$ at $P_o(Cl_2) = 600$ torr yielded equivalent angular distributions. Figure 6 also emphasizes the absence of even approximate symmetry about $\Theta = 0°$ in the scattered signal; this $\Theta < 0°$ angular range was inaccessible in later experiments (III-V) where the TOF pulsing wheel had been installed. Figure 8 is included in order to demonstrate that the small Θ peaking observed in Exps. I-III was not an experimental artifact arising from the choice of the Cl_2 beam as the modulated beam. Small quantitative differences between results of Exps. III and IV are discussed in a later section. Results of Exp. V shown in Fig. 9 illustrate the universality of the phenomenon, i. e. the same qualitative features appear in the $Br_2 + (Cl_2)_x$ and $Br_2 + (NH_3)_x$ systems. In this connection, the angular distribution of the $C_2H_4Cl_4^+$ signal in a brief examination of $C_2H_4 + (Cl_2)_x$ also peaked sharply in this small, positive Θ region.

Predicted Condensate Angular Distributions

The shapes and insensitivity to mass examined of the angular distributions of Figs. 6-9 are all consistent with the general bimolecular condensation mechanism, reaction (R6). By momentum conservation, the AB_x^* product of this reaction must be formed with a LAB velocity equal to the velocity of the center of mass of the A and B_x reactants, C_x(the centroid). Thus, AB_x^* would appear at a LAB scattering angle given by

$$\theta_c = \arctan(\gamma/x) \tag{4}$$

with $\gamma = m_A v_A / m_B v_x$ in terms of the masses of A and B monomer and the speeds of A and B_x (assumed independent of x in this treatment). The interpretation of the $BrCl^+$ angular distribution in Fig. 6, for example, is that a distribution in x in the $(Cl_2)_x$ beam resulted in $Br_2(Cl_2)_x^*$ complexes which scattered at the θ_c values given by Eq. (4) and partially fragmented into $BrCl^+$ upon EB ionization.

Figures 2 and 3 suggest that the $(Cl_2)_x$ is not strongly condensed, i. e. that the flux in the beam corresponding to a given cluster decreases with increasing x. In view of this, it is important to examine the product intensity expected from this model carefully in order to understand the observed product angular distribution peaking near $\Theta = 0°$. The number of AB_x^* products of reaction (R6) formed per second is

$$N(x) = Vg\Omega_c(x)\, F_A F_x / v_A v_x \tag{5}$$

in terms of the volume of the BIR, V, the relative collision speed, $g = (v_A^2 + v_x^2)^{1/2}$, the cross section for reaction (R6), $\Omega_c(x)$, and the fluxes of A and B_x at the BIR, F_A and F_x. If the angular and speed distributions of both beams were delta functions, all of the AB_x^* would recoil at a particular θ_c given by Eq. (4). This would produce a measured AB_n^+ signal of

$$S_n(x) = KT(nm_B + m_A)h_{n,x}\Omega_c(x)F_x\Omega_i(AB_x). \tag{6}$$

Here, T is the transmission of the ion optics and quadrupole mass filter, dependent weakly on the mass of the detected ion; $\Omega_i(AB_x)$ is the AB_x^* EB ionization cross section; $h_{n,x}$ is the fragmentation probability, the probability that AB_n^+ is formed upon EB ionization of AB_x^*; and

$K = V_g F_A \ell j / v_A v_x e C_x$ is an approximate constant during one experiment (j = electron current density in ionizer of lenth ℓ; e = charge on the electron). Equation (6) already predicts that scattered signal should be seen only at $\Theta > 0°$ in approximate agreement with Figures 1 and 6. Owing to finite apparatus angular resolution, however, recoil distributions of neighboring AB_x^* condensates overlap so that x is to be treated as a continuous variable. This produces an angular distribution of AB_n^+ massfilter signal given by

$$I_n(\Theta) = S_n(x) \left| dx/d\theta_c \right| = \gamma K T(nm_B + m_A) h_{n,x} Q_c(x) F_x Q_i(AB_x) \sin^{-2}\Theta \qquad (7)$$

where the Jacobian factor, $\left| dx/d\,\theta_c \right|$, is given by $\gamma/\sin^2\Theta$.

The quantity of most interest in Eq. (7), $Q_c(x)$, cannot be extracted from the data because of the uncertain form of F_x. Nevertheless, information on some of the parameters in Eq. (7) can be obtained from the data. For example, the ratio of angular distributions measured for two different massfilter settings in one experiment yields

$$R_{n',n}(x) = \frac{I_{n'}(\Theta)}{I_n(\Theta)} = \frac{T(n'm_B + m_A) h_{n',x}}{T(nm_B + m_A) h_{n,x}} \,. \qquad (8)$$

Table II gives $R_{n',n}(x)$ values measured in Exps. III and V. These data were obtained at approximately constant quadrupole resolution ($\Delta m/m$) setting and $T(m)$ might have favored higher m slightly. Thus, the heavy AB_x^* clusters clearly fragment into small ionic fragments. Indeed, the data indicate that $h_{n,x}$ peaks at $n \approx 1$ and that the fragmentation pattern at low n is approximately independent of x (at least for $Br_2(Cl_2)_x^*$). However, the data give no indication whether a second, larger peak in $h_{n,x}$ might occur near the n = x end of the spectrum. Nevertheless, this provided the first suggestion that extrapolation of the mass spectra of the

main beam itself, such as are shown in Figs. 2 and 3, might underestimate the concentration of heavier clusters.

The $\sin^{-2}\Theta$ Jacobian factor in Eq. (7) represents a very strong weighing factor favoring small Θ scattering. Furthermore, other factors in Eq. (7) favor large x and small Θ as well. As discussed earlier, $Q_i(AB_x)$ should be roughly proportional to x. It is unlikely that $Q_c(x)$ would decrease with increasing x above some critical size, x_c, where decomposition of AB_x^* is no longer important. For $x > x_c$, it seems reasonable to expect $Q_c(x) \alpha x^t$ for $t \approx 0\text{-}2/3$; the $t = 2/3$ limit corresponds to a geometric cross section and is probably the most reasonable estimate. In summary, then, the $Q_c(x)Q_i(AB_x) \sin^{-2}\Theta$ factors in Eq. (7) favor small angle scattering approximately as $\Theta^{-t-3} \approx \Theta^{-11/3}$. This is a very strong weighing factor; $h_{n,x}F_x$ must fall-off with increasing x faster than $x^{-11/3}$ in order to prevent $I_n(\Theta)$ from peaking at $\Theta = 0°$.

Figure 10 shows plots of $h_{n,x}F_x \alpha \tan^{5/3}\Theta \sin^2\Theta I_n(\Theta)$ versus $x = x(\theta_c)$. Similar plots of $\tan\Theta \sin^2\Theta I_n(\Theta)$ (corresponding to $Q_c(x)$ = constant) show only a slightly steeper fall-off with increasing x. It is also unlikely that $h_{n,x}$ for small n would increase rapidly with increasing x. In the simplest statistical picture, in fact, $h_{n,x}$ might be expected to vary simply as x^{-1} due to the increasing range in n, especially in view of the approximate invariance of the fragmentation patterns of Table II with changing x. Thus, it is likely that F_x decreases with increasing x roughly as is shown in Fig. 10. This is especially important because the rate of decrease in F_x with increasing x for the data of Exp. III is much slower in Fig. 10 than in Fig. 3. Writing $F_x = A \exp[-\beta x]$, for example, $\beta = 0.43$ is obtained from Fig. 3 whereas $\beta = 0.105$ is obtained from the data of Exp. III in Fig. 10.

This provides stronger proof of the comment made in reference to Table II that extrapolation of the mass spectrum of the nozzle beam, uncorrected for fragmentaion, seriously underestimates the concentration of heavier clusters. Indeed, analysis of scattered angular distributions, such as are presented here, in terms of Eq. (7) should provide the most reliable method of measuring the concentration of these moderately heavy clusters (i. e., $10\text{-}20 \leq x \leq 100\text{-}200$) in the nozzle beam.

The interpretation of the $\tan^{5/3}\Theta \sin^2\Theta I_n(\Theta)$ plots in Fig. 10 as being proportional to $h_{n,x}F_x$ must fail at small $x<x_c$ because the AB_x^* cannot be expected to live long enough to reach the detector. The likely lifetime, τ, of an AB_x^* can be estimated very crudely from the classical expression,

$$\tau\,(\text{sec}) \approx 10^{-13}[(\epsilon - \epsilon_o)/\epsilon]^{7-3N} \qquad (9)$$

where N is the number of heavy atoms in the cluster. For $Br_2^+(Cl_2)_x$ in Exp. III, for example, the relative collision energy was 5.8 kcal/mole (large x limit) and $\tau > 0.7 \times 10^{-3}$ sec was required in order that the $Br_2(Cl_2)_x$ complex reach the ionizer before decomposition. King, et. al.[7] estimate the Cl_2 - Cl_2 bond energy at ~ 1 kcal/mole. Since reaction (R4) represents the adsorption of Br_2 on a Cl_2 surface, ϵ_o might be estimated at ~ 3 kcal/mole. If these parameters are inserted into Eq. 9, a minimum number of heavy atoms in the cluster of $N \approx 20$ is obtained. It is interesting to note that data of the three experiments shown in Fig. 10 all exhibit breaks (i. e., deviations from the limiting high x behavior) in the vicinity of 20-25 heavy atoms in the cluster. This makes the assignment of the high x behavior observed here to the general condensation reaction (R6) even more plausible.

TOF Spectra of Scattered Signal

In order to demonstrate even more clearly the assignment of the measured angular distributions to reactions (R4) and (R5), TOF spectra of the scattered signals were measured [9a] in Exps. III, IV, and V. Since the conclusions from the $(Cl_2)_x$ and $(NH_3^{\cdot})_x$ data were the same, only data on $Br_2 + (Cl_2)_x$ is presented here in Figs. 11 and 12.

In interpretating the TOF data, perfect apparatus angular resolution has been assumed. If both beams were monoenergetic, a particular $Br_2(Cl_2)_x^*$ condensate of reaction (R4) would be found with a unique LAB velocity. Owing to the small but finite spread in actual beam speeds (Table I), however, this same $Br_2(Cl_2)_x$ condensate is formed with a small spread in LAB scattering angle and speed. The distributions for different $Br_2(Cl_2)_x$ were easily calculated as a function of Θ, $I(\Theta, v, x)$, from the measured beam speed distributions by means of the formalism developed in Ref. 12 (assuming $Q_c(x)$ to be independent of g). These were normalized such that

$$\int I(\Theta, v, x)\, d\Theta\, dv = 1. \tag{10}$$

Finally, a composite LAB recoil speed distribution for a given mass filter setting was calculated from

$$I_n(\Theta, v) = \sum_x x^{5/3} h_{n,x} F_x I(\Theta, v, x) \tag{11}$$

with $h_{n,x}F_x$ given in Fig. 10. It is perhaps also worth emphasizing that major contributions to a given Θ came from a small range in x; for Exp. III, for example, x = 18-22 accounted for 77% of the $\Theta = 5°$ peak intensity, x = 9-11 accounted for 89% of the $\Theta = 10°$ peak intensity. Finally, $I_n(\Theta, v)$ was convoluted over the TOF pulsing wheel gate function and ionizer

length and normalized to unit peak height at a given Θ for comparison with the TOF data.

Figures 11 and 12 show that the fits to the data provided by Eq. (11) are surprisingly good. Clearly, reaction (R4) accounts for the dominant features of all of the $Br_2 + (Cl_2)_x$ data presented here. As in Fig. 4, most of the breadth in the TOF spectra of Figs. 11 and 12 is instrumental. Figure 13 shows that the actual calculated speed distribution is very narrow. This figure also shows the corresponding $Br_2 + (NH_3)_x$ speed distributions calculated for reaction (R5) from Eq. (11) which provided an equally good fit to the TOF spectra measured in Exp. V.

Although the qualitative results of Exps. II, III, and IV were the same, some quantitative differences are apparent. Thus, the data of Fig. 5 show a steeper small Θ rise of the product angular distribution as $P_o(Cl_2)$ increases due to the increasing condensation of the nozzle beam. A hint of this same effect appears in the slight broadening of the $\Theta = 5°$ TOF spectra recorded in Exp. II for $P_o(Cl_2) = 450$ torr. Experiments III and IV were conducted with constant P_o, T_o, and d parameters for the Cl_2 nozzle. Nevertheless, comparison of Figs. 7 and 8 indicate that the Cl_2 nozzle contained a higher concentration of heavy clusters in Exp. III. This is particularly apparent in Fig. 10 where the straight line fits to the $h_{n,x}F_x$ data points yield exponential slope parameters, β, of 0.105 (Exp. III) and 0.124 (Exp. IV). This result indicates that the geometry of the nozzle throat influences the degree of condensation, with the slower expansion through the longer throat in Exp. III producing stronger condensation. This trend with changing nozzle geometry observed here parallels that reported in Ref. 3 where expansion through

a sonic nozzle produced less condensation than did expansion through a conical nozzle. Comparison of $\Theta = 10°$ TOF data in Figs. 11 and 12 also illustrate this same point with the Exp. IV results (especially for $BrCl^+$) broadened and shifted to slower LAB speeds relative to the calculated centroid distributions. This clearly shows the effect of decomposition of some of the lighter AB_x^* complexes. Although there are too many variables and insufficient data to characterize this decomposition, auxiliary calculations [9a] simulating the $\Theta = 10°$ TOF spectra based on the decomposition of some lighter clusters corresponding to $\theta_c > 10°$ (Eq. (4)) did reproduce this broadening towards lower LAB recoil speeds.

DISCUSSION

In summary, condensation of a Br_2 probe particle on heavy $(Cl_2)_x$ or $(NH_3)_x$ has been described here. In agreement with observations in Ref. 8 on reaction (R3), product angular distributions are sharply peaked near the cluster beam. Indeed, this sharp peaking at small but positive Θ should be a general characteristic of such condensation reactions. In scattering studies employing crossed nozzle beams, the nozzle stagnation pressures are typically as high as possible in order to enhance beam intensity and nozzle speed characteristics. As has been emphasized earlier [13], however, care must be taken to insure that features of the measured distribution have not been influenced by clusters in the beam. In view of the tendency of heavier clusters to fragment upon EB ionization which is observed here, the best test against such cluster participation is to demonstrate insensitivity of any small angle peak shapes in the measured angular distribution to nozzle stagnation pressures.

It is also of interest to inquire how studies reported here and in Ref. 8 can be improved so as to resolve the dynamics of condensation and possible subsequent decomposition as a function of cluster size. Much more information could be obtained if apparatus resolution were sufficient to resolve peaks in LAB (Θ, v) space due to individual values of x (e.g., Eq. (6) rather than Eq. (7)). This might be achieved by improving the kinematics through an increase in the γ factor of Eq. (4). In this regard, the use of Br_2 as the probe particles in these studies rendered m_A about as large as possible consistent with the present experimental arrangement where the nozzle gas must be admitted to the stagnation chamber through an unheated gas inlet tube. The mass of the cluster monomer unit, m_B, was also rendered as small as experimentally feasible through the use of NH_3; an attempt to generate an $(H_2)_x$ cluster beam failed because the nozzle stagnation chamber could not be cooled below 77°K. Another approach to increasing γ would be to increase v_A; this could probably best be achieved in an ion-molecule scattering study.

In addition to improved kinematics through a larger γ factor, it should be possible to resolve the reactions of the smaller clusters by a careful study of the dependence of the scattered distributions on the pressure and temperature of the nozzle stagnation chamber, especially in view of the results of Ref. 3 that the degree of condensation depends upon $P_o T_o^{\ C_P/(C_V-C_P)}$. King, Dixon, and Herschbach[7] attributed their measurements of the angular and TOF distributions of the $BrCl^+$ signal from crossed Br_2 and Cl_2 nozzle beams to reaction (R1). Their Cl_2 nozzle stagnation chamber conditions (P_o = 500 torr, T_o = 290°K, d = 0.0075 cm[14]) appear only

slightly less conducive to condensation that those employed in Exp. II so that the differing chemical phenomena reported in these two studies warrants comment. Comparison of reported nozzle expansion conditions could be misleading because clogging or erosion of the nozzle throat could significantly alter the nozzle diameter in either study. Unfortunately, a high mass-independent background in the present study precluded the use of lower Cl_2 stagnation pressures in an attempt to seek out the transition between the scattering phenomena reported here and in Ref. 7. More recently, however, Dixon and Herschbach[15, 16] have observed the beginning of this transition by measuring the scattering as a function of $P_o(Cl_2)$ and resolving reactions of Br_2 with $(Cl_2)_2$, $(Cl_2)_3$, and $(Cl_2)_4$.

Another exciting possibility suggested by the results presented here is the preparation of beams of heavy clusters of sharply defined molecular weight by means of a small orifice which could be rotated about the BIR defined by the nozzle beams employed here. This orifice would then transmit AB_x with x determined through Eq. (4) by the angular position of the orifice. The transmitted AB_x beam should be of sufficient intensity to permit measurements of the dependence on size of many properties of the AB_x complex (e. g., ionization potential, EB ionization cross sections, fragmentation patterns, etc.).

ACKNOWLEDGMENT

All data reported here was collected while this program was supported by the USAEC through the Lawrence Berkeley Laboratory. The final interpretative phase was conducted at the Ames Laboratory and supported by the USERDA under contract No. W-7405-eng-82. We also wish to thank D. A. Dixon and D. R. Herschbach for making their recent results known to us prior to publication.

REFERENCES

1. R. E. Leckenby, E. J. Robbins, and P. A. Trevalion, Proc. Roy. Soc. (London) 280A, 409 (1964). This reference also reviews earlier reports of the phenomenon.
2. F. T. Green and T. A. Milne, J. Chem. Phys. 39, 3150 (1963); T. A. Milne and F. T. Green, J. Chem. Phys. 47, 4095 (1967).
3. O. F. Hagena and W. Obert, J. Chem. Phys. 56, 1793 (1972).
4. B. Raoult and J. Farges, Rev. Sci. Instr. 44, 430 (1973); J. Farges, B. Raoult, and G. Torchet, J. Chem. Phys. 59, 3454 (1973).
5. W. Henkes and F. Mikosch, Int. J. Mass. Spect. Ion Phys. 13, 151 (1974).
6. J. Gspann and G. Krieg, J. Chem. Phys. 61, 4037 (1974).
7. D. L. King, D. A. Dixon, and D. R. Herschbach, J. Am. Chem. Soc. 96, 3328 (1974).
8. A. Gonzalez Urena, R. B. Bernstein, and G. R. Phillips, J. Chem. Phys. 62, 1818 (1975).
9. (a) R. Behrens, Jr., Ph. D. thesis, University of California, Berkeley (1975); (b) R. Behrens, Jr., A. Freedman, R. R. Herm, and T. P. Parr, "Elastic Differential Cross Sections and Intermolecular Potentials for Ar + CH_4 and Ar + NH_3" (to be published).
10. This was purchased from Buckbee Mears Company, St. Paul, Minn.
11. F. W. Lampe, J. L. Franklin, and F. H. Field, J. Am. Chem. Soc. 79, 6129 (1957).
12. C. A. Mims, S.-M. Lin, and R. R. Herm, J. Chem. Phys. 57, 3099 (1972).

13. H. J. Dittmers, Ch. Shutze, B. Fischer, and K. Schügerl, Z. Physik. Chem. Neue Folge 80, 220 (1972).

14. The nozzle diameter is not quoted in Ref. 7 but was taken from Ref. 15.

15. D. A. Dixon, Ph. D. thesis, Harvard University, Cambridge, Mass. (1975).

16. D. A. Dixon and D. R. Herschbach, "Molecular Beam Chemistry: Reactions Exchanging van der Waals Bonds Among Three or More Halogen Molecules" (to be published).

Table I. Experimental nozzle beam conditions.

Experiment	Beam Source	Beam Species	T (°K)	P_o (torr)	y[a] (cm)	Speed distribution[b] u	α
	1	$(Cl_2)_x$	298	780	1.2	—	—
I	2	Br_2	298	250	0.87	—	—
	1	$(Cl_2)_x$	298	Varied	0.71	—	—
II	2	Br_2	323	260	0.56	—	—
	1	$(Cl_2)_x$	298	700	0.71	440	29.5
III	2	Br_2	323	260	0.56	331	49.4
	1	Br_2	323	260	0.56	336	36.6
IV	2	$(Cl_2)_x$	298	700	0.64	400	29.5
	1	Br_2	323	260	0.56	336	36.6
V	2	$(NH_3)_x$	298	700	0.64	900	72.8

[a] y is the nozzle-skimmer distance. The diameter, external angle, and internal angle of the skimmer was: 0.16 cm, 64°, 50° (Beam 1) and 0.051 cm, 64°, 50° (Beam 2) in Exp. I; 0.050 cm, 64°, 50° (Beam 1) and 0.062 cm, 86°, 60° (Beam 2) in all other experiments.

[b] Parameters of Eq. (2) in m/sec obtained by deconvolution of TOF spectra measured for the nozzle beam. Parameters quoted for cluster beams were measured for largest $(Cl_2)_n^+$ or $(NH_3)_n^+$ TOF spectra which provided reasonable signal-to-noise; n = 6, 3, and 6 for Exps. III, IV, and V, respectively. All neutral clusters are assumed to have this speed distribution in centroid calculations.

Table II. Fragmentation Pattern Estimates for AB_x^* Ionization formed in $A + B_x \rightarrow AB_x^*$.[a]

$Br_2 + (Cl_2)_x \rightarrow Br_2 \cdot (Cl_2)_x^*$			
θ	5°	7°	10°
x	19.7	14.0	9.8
$R_{2,2}$	1.00	1.00	1.00
$R_{3,2}$	0.67	0.69	0.78
$R_{4,2}$	0.21	0.20	—
$R_{5,2}$	0.23	0.31	0.33

$Br_2 + (NH_3)_x \rightarrow Br_2 \cdot (NH_3)_x^*$				
θ	5°	7°	9°	11°
x	39.8	28.4	22.0	17.9
$R_{1,1}$	1.00	1.00	1.00	1.00
$R_{2,1}$	0.78	1.52	1.59	1.11
$R_{3,1}$	0.47	0.55	0.59	0.70
$R_{5,1}$	0.36	0.40	0.04	0.04

[a] $R_{n',n}$ is defined in Eq. (8). Data from Exp. III and V.

FIGURE CAPTION

Fig. 1. Angular distribution of neutral species scattered from crossed nozzle beams of Br_2 and $(Cl_2)_x$ measured for a $BrCl^+$ massfilter setting. Beam conditions listed in Table I as Exp. I. Solid data symbols (here and elsewhere) indicate that measured signal was less than 0.33 counts/second.

Fig. 2. Solid curve shows mass spectrum of Cl_2 nozzle (beam 1) recorded in an early experiment (not listed in Table I) with P_o = 500 torr and T_o = 298°K. Data symbols show mass spectra of scattered species, obtained in Exps. I and III, arbitrarily normalized to 80% peak heights.

Fig. 3. Data points show the relative intensities of different Cl_n^+ signals in the mass spectrum of the Cl_2 nozzle of Exp. III.

Fig. 4. Data symbols show measured TOF spectra of the Cl_2 nozzle of Exp. III obtained for different Cl_n^+ massfilter signals. Solid curve shows a fit of Eqs. (2) and (3) to the Cl_2^+ data. Signals for differing n are arbitrarily normalized for ease of visual presentation. Convention for TOF data here and elsewhere is to measure time from the instant that the TOF pulsing wheel begins to transmit molecules. This TOF pulsing wheel's gate-function was: square, 90 μsec wide for Fig. 4; trapezoidal, 158 μsec full-width, 22 μsec width at peak transmission for Figs. 11 and 12.

Fig. 5. Angular distributions measured in Exp. II at the $BrCl^+$ mass-filter setting.

Fig. 6. Angular distributions from Exp. I measured for $BrCl^+$, $Br_2Cl_2^+$, $Br_2Cl_4^+$, and $Br_2Cl_8^+$ massfilter settings. Scales alternate from left to right for different species starting from the top left for $BrCl^+$.

Fig. 7. Angular distributions from Exp. III measured for $BrCl^+$, $Br_2Cl_4^+$, $Br_2Cl_6^+$, $Br_2Cl_8^+$, $Br_2Cl_{10}^+$ massfilter settings. Measured number densities are shown in arbitrary units. Absolute counts at $\Theta = 5°$ in the standard 120 second counting period were: $BrCl^+ = 2500$; $Br_2Cl_4^+ = 6400$; $Br_2Cl_6^+ = 4300$; $Br_2Cl_8^+ = 1320$; and $Br_2Cl_{10}^+ = 1480$.

Fig. 8. Angular distributions from Exp. IV for $BrCl^+$, $Br_2Cl_2^+$, $Br_2Cl_6^+$, and $Br_2Cl_{10}^+$ massfilter settings. Scale convention as in Fig. 6.

Fig. 9. Angular distributions from Exp. V for $BrNH_3^+$, $Br_2(NH_3)_2^+$, $Br_2(NH_3)_3^+$, and $Br_2(NH_3)_5^+$ massfilter settings. Scales alternate from left to right starting with $Br(NH_3)^+$ at top left.

Fig. 10. Plot of $\sin^2 \Theta \tan^{5/3} \Theta\, I(\Theta)$ (in arbitrary units) versus $x = x(\Theta)$ (Eq. (4)). Discussion in text shows that this amounts to a plot of $h_{n,x}F_x$ (parameters of Eq. (7)) versus x. Data for different massfilter settings (i.e., n) from a given experiment has been normalized to each other. Upper $Br_2 + (Cl_2)_x$ data from Fig. 7, lower from Fig. 8 ; $Br_2+(NH_3)_x$ data from Fig. 9 .

Fig. 11. Data symbols show TOF spectra of scattered signals at different massfilter settings measured in Exp. III at $\Theta = 5°$ and $10°$. Also shown at $\Theta = 5°$ are TOF spectra of $BrCl^+$(●) and $Br_2Cl_6^+$ (◆)

measured in Exp. II at $P_o(Cl_2) = 450$ torr. The solids curves are calculated TOF spectra (Eq. (11)) for products of reaction (R4).

Fig. 12. TOF spectra of scattered signals from Exp. IV; conventions as for Fig. 11.

Fig. 13. Velocity vector diagrams for $Br_2 + (Cl_2)_x$ (Exp. III) and $Br_2 + (NH_3)_x$ (Exp. V). Beam flow velocities (Table I) are depicted along with relative collision velocity, g, and centroid velocities, C. Subscripts on C denote x values which would correspond (Eq. (4)) to AB_x^* (reactions (R4) and (R5)) recoil at a particular Θ. Also shown along each Θ = constant line are AB_x^* product speed distributions calculated as described in the text from Eq. (11). Relative peak heights versus Θ are arbitrary for ease of visual presentation.

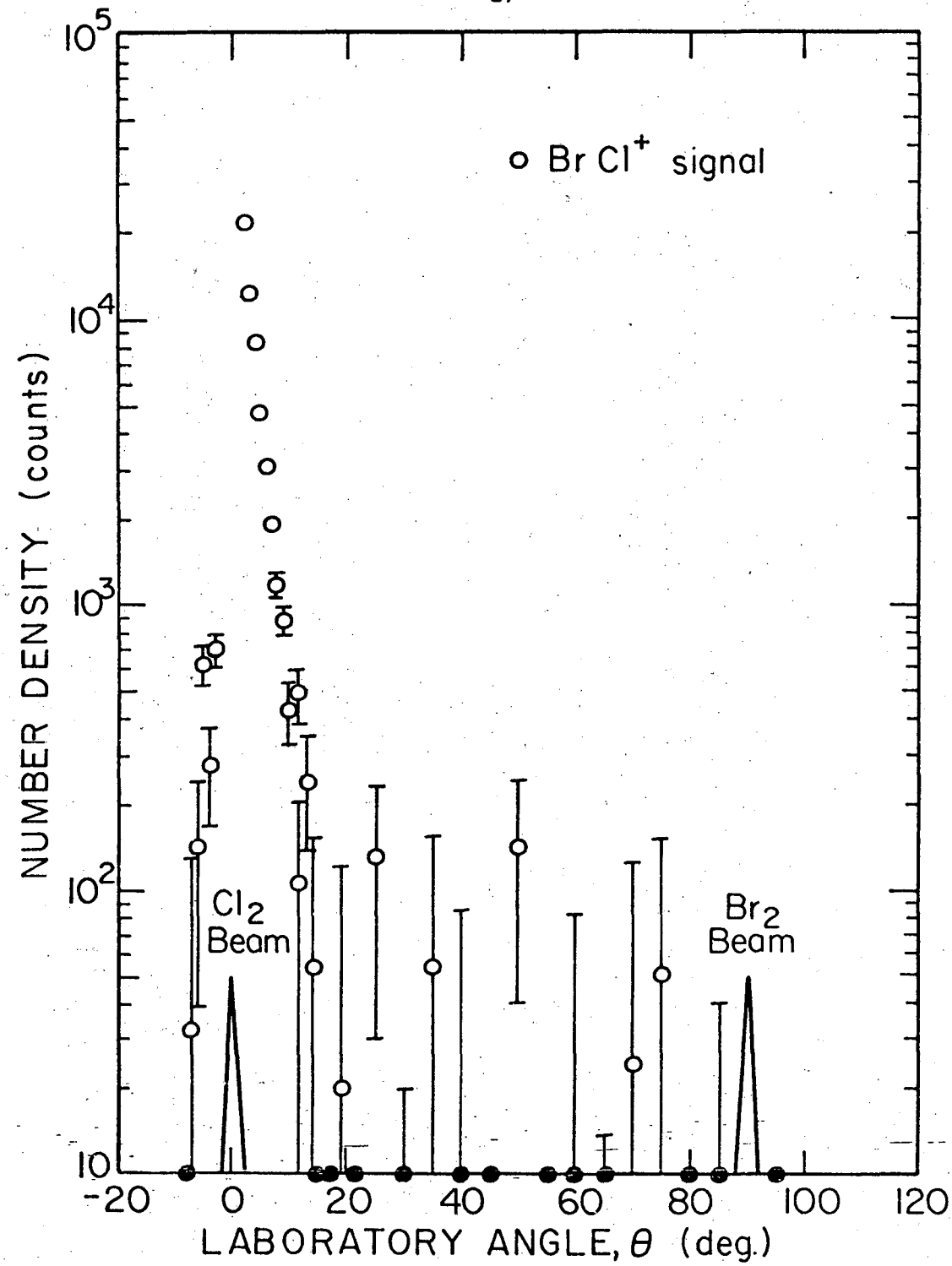

XBL756-6500

Fig. 1

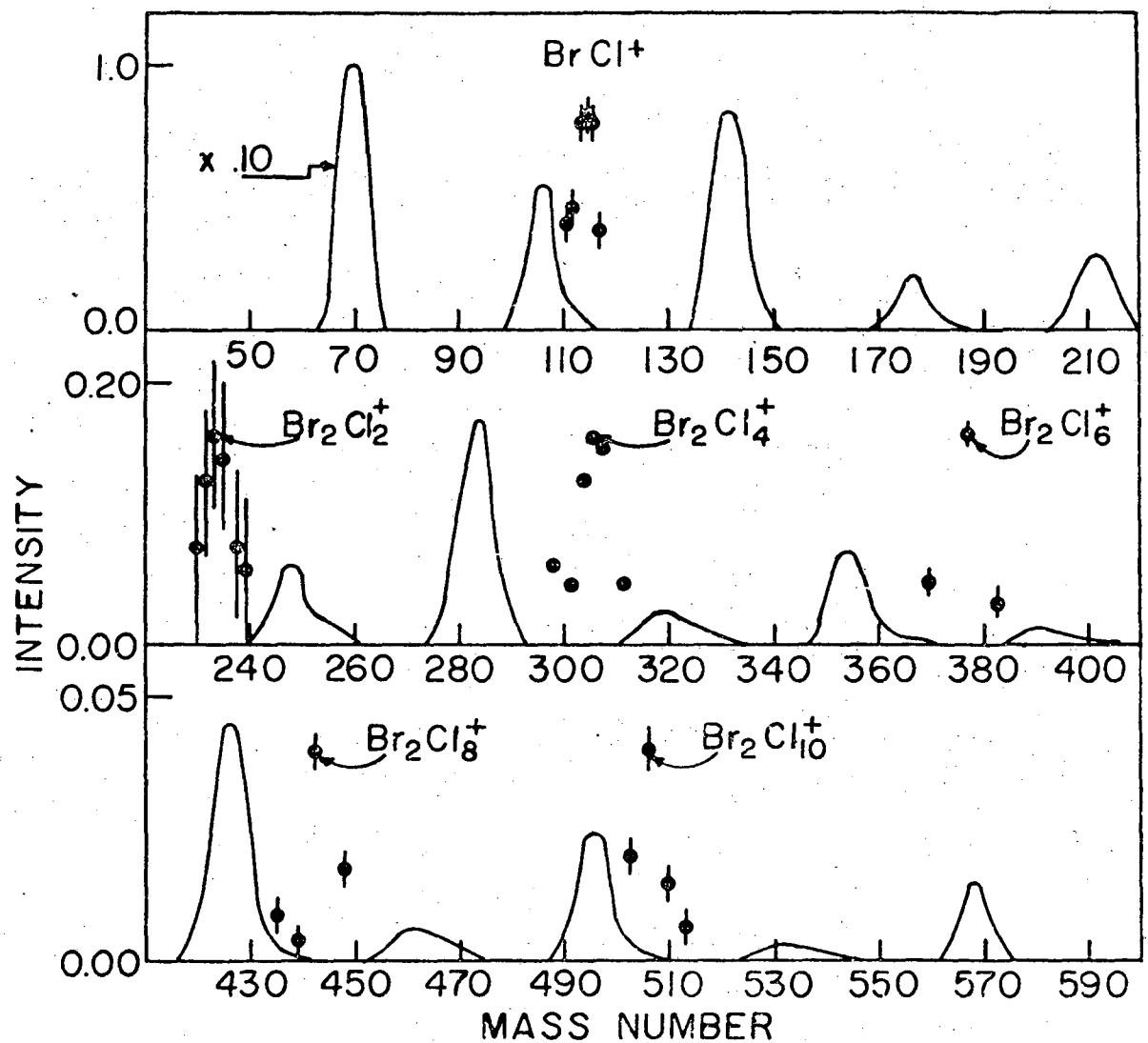
BrCl+
x .10
1.0
0.0
50 70 90 110 130 150 170 190 210
0.20
0.00
Br2Cl2+
Br2Cl4+
Br2Cl6+
240 260 280 300 320 340 360 380 400
0.05
0.00
Br2Cl8+
Br2Cl10+
430 450 470 490 510 530 550 570 590
INTENSITY
MASS NUMBER

Fig. 2

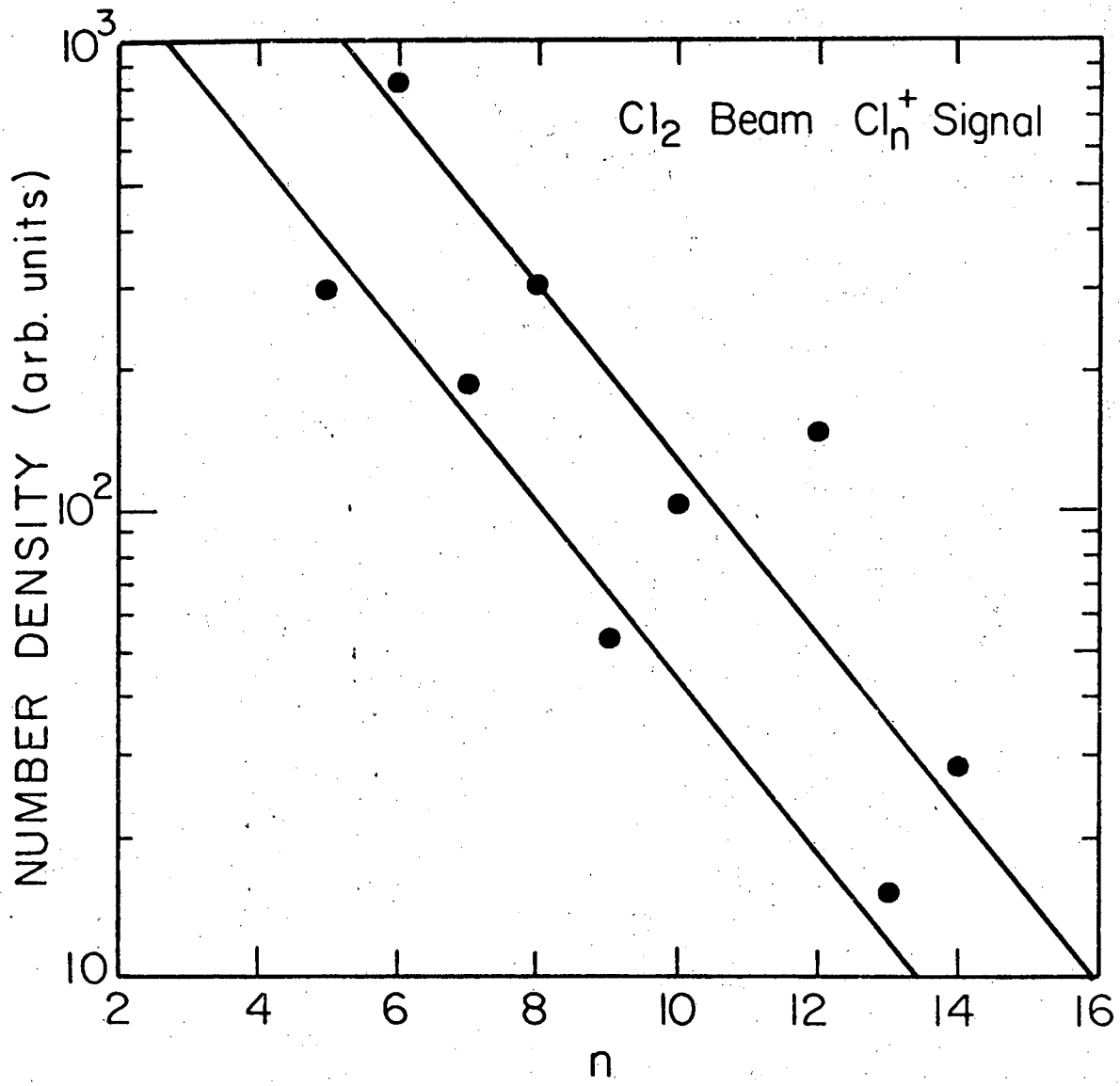

XBL 756-6503

Fig. 3

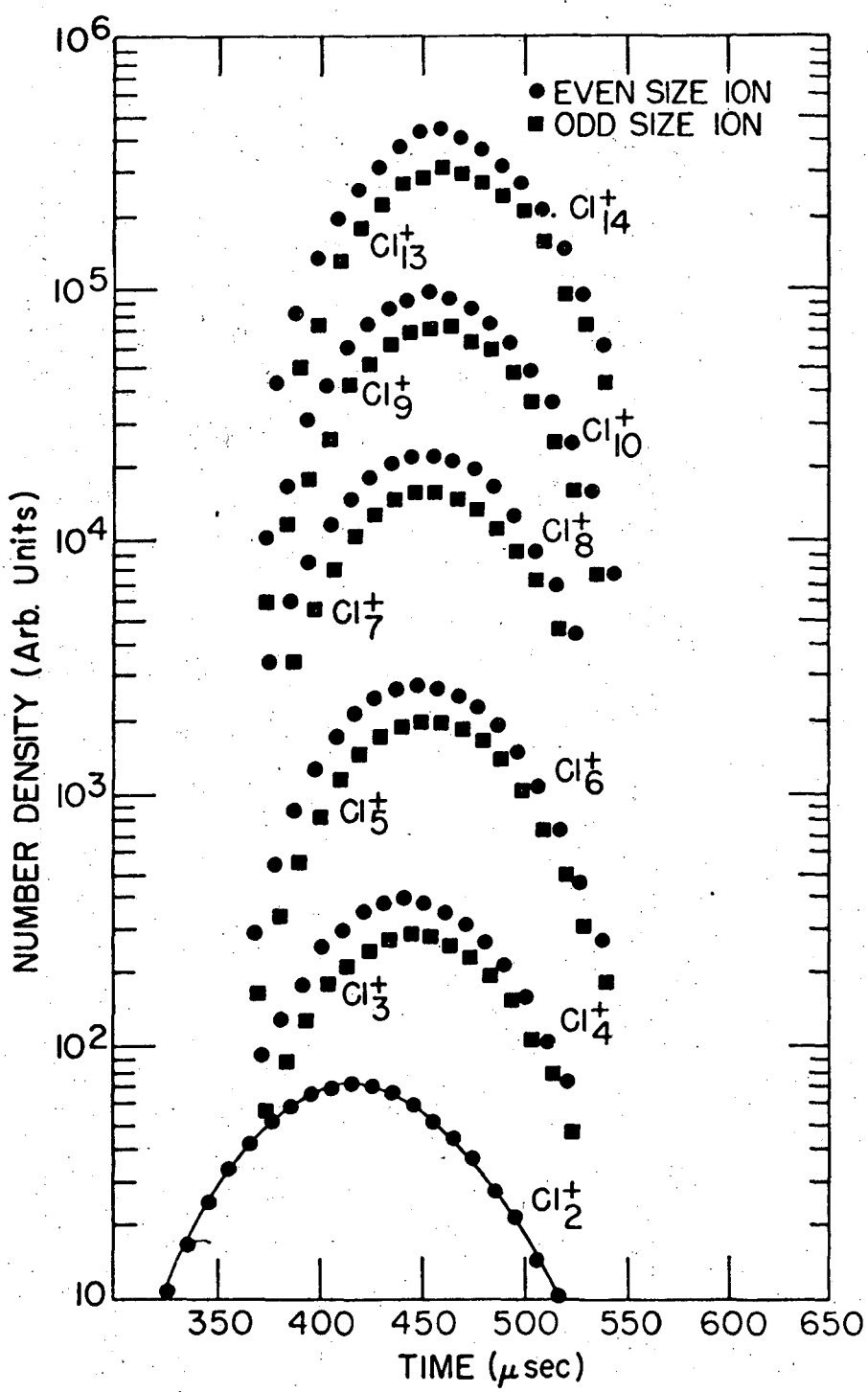
EVEN SIZE ION
ODD SIZE ION
Cl_{14}^+
Cl_{13}^+
Cl_9^+
Cl_{10}^+
Cl_8^+
Cl_7^+
Cl_6^+
Cl_5^+
Cl_3^+
Cl_4^+
Cl_2^+
10^6
10^5
10^4
10^3
10^2
10
NUMBER DENSITY (Arb. Units)
350
400
450
500
550
600
650
TIME (μsec)

Fig. 4

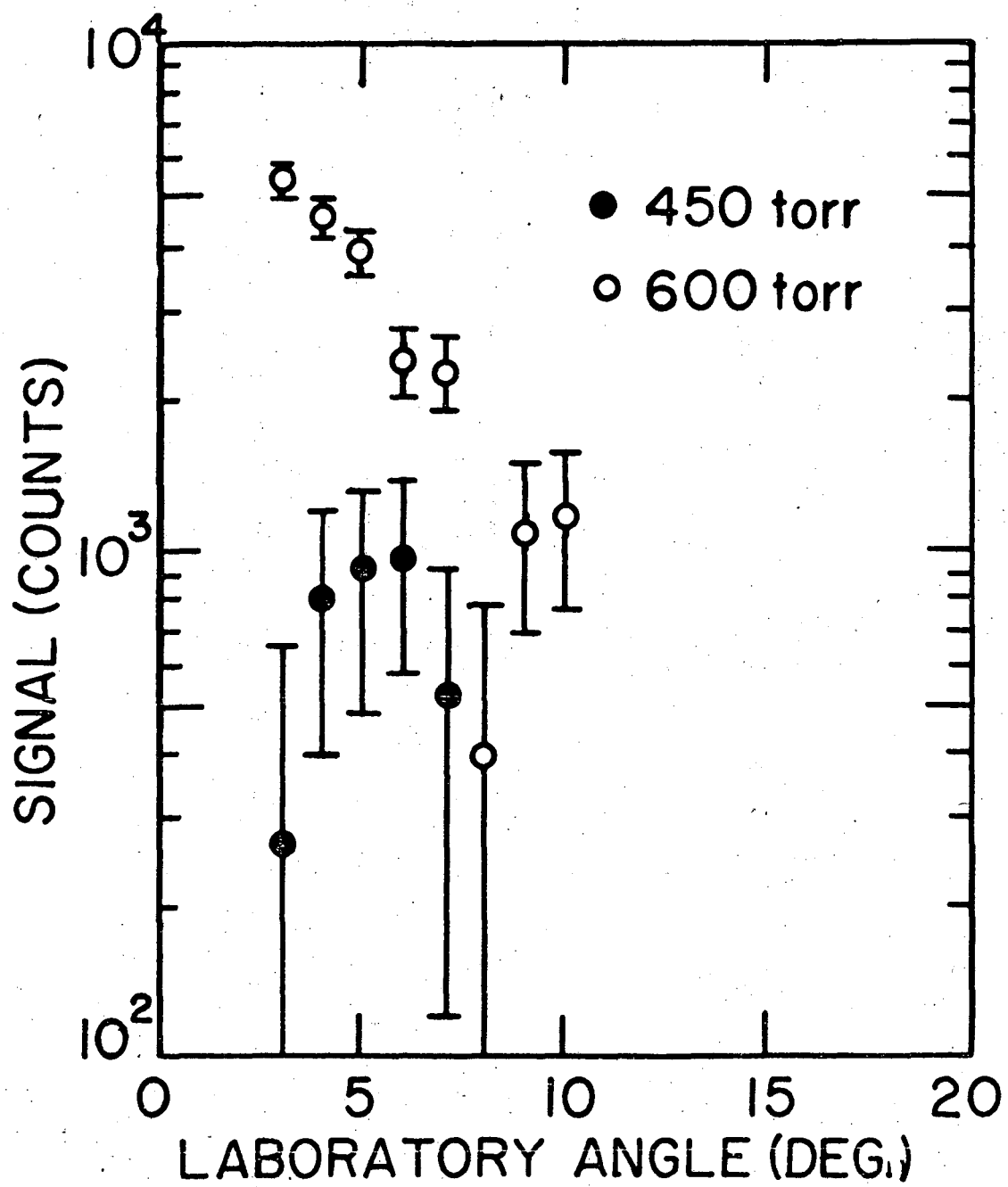
10^4
10^3
10^2
SIGNAL (COUNTS)
450 torr
600 torr
0
5
10
15
20
LABORATORY ANGLE (DEG.)

Fig. 5

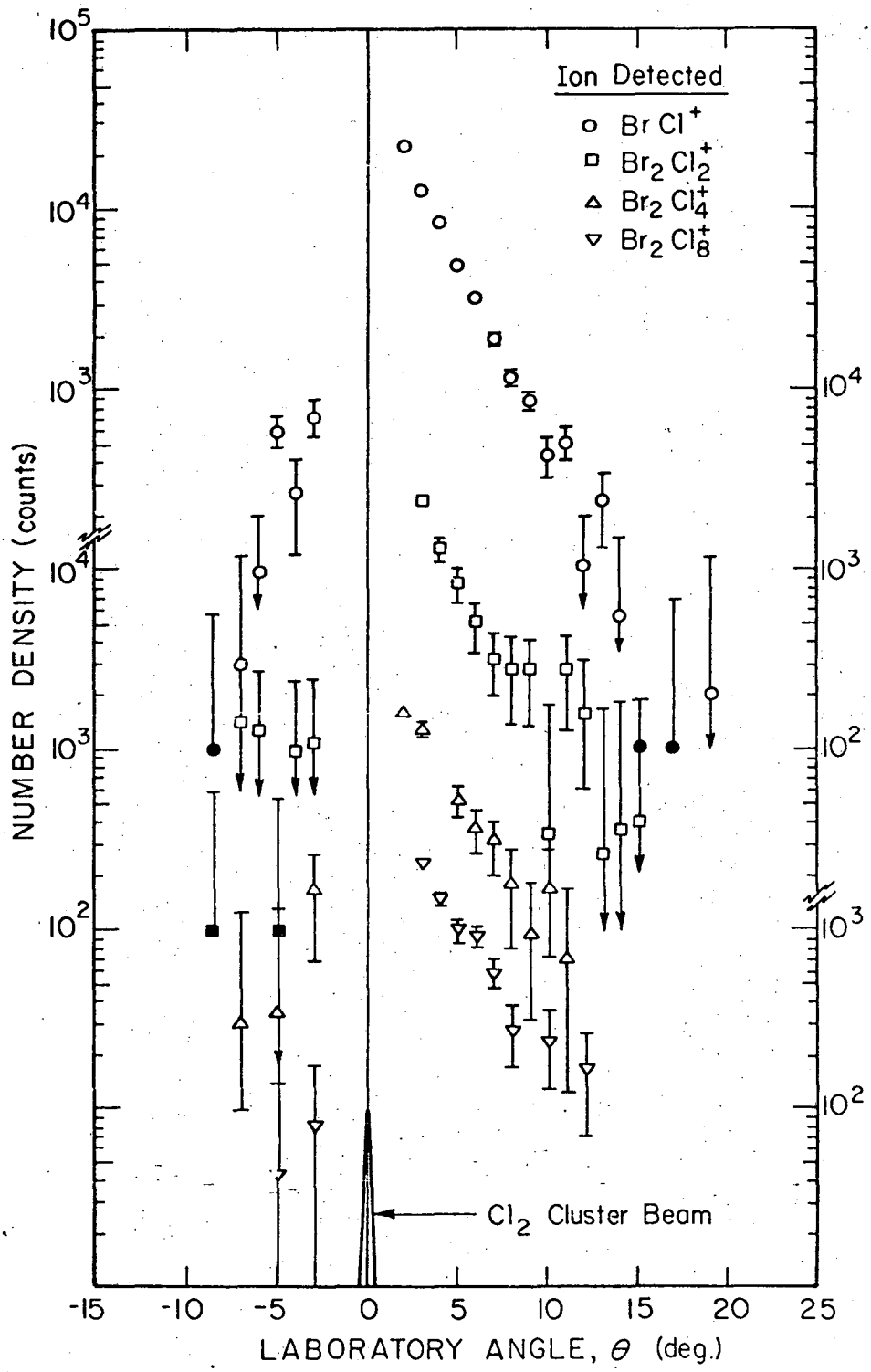

XBL 756-6505

Fig. 6

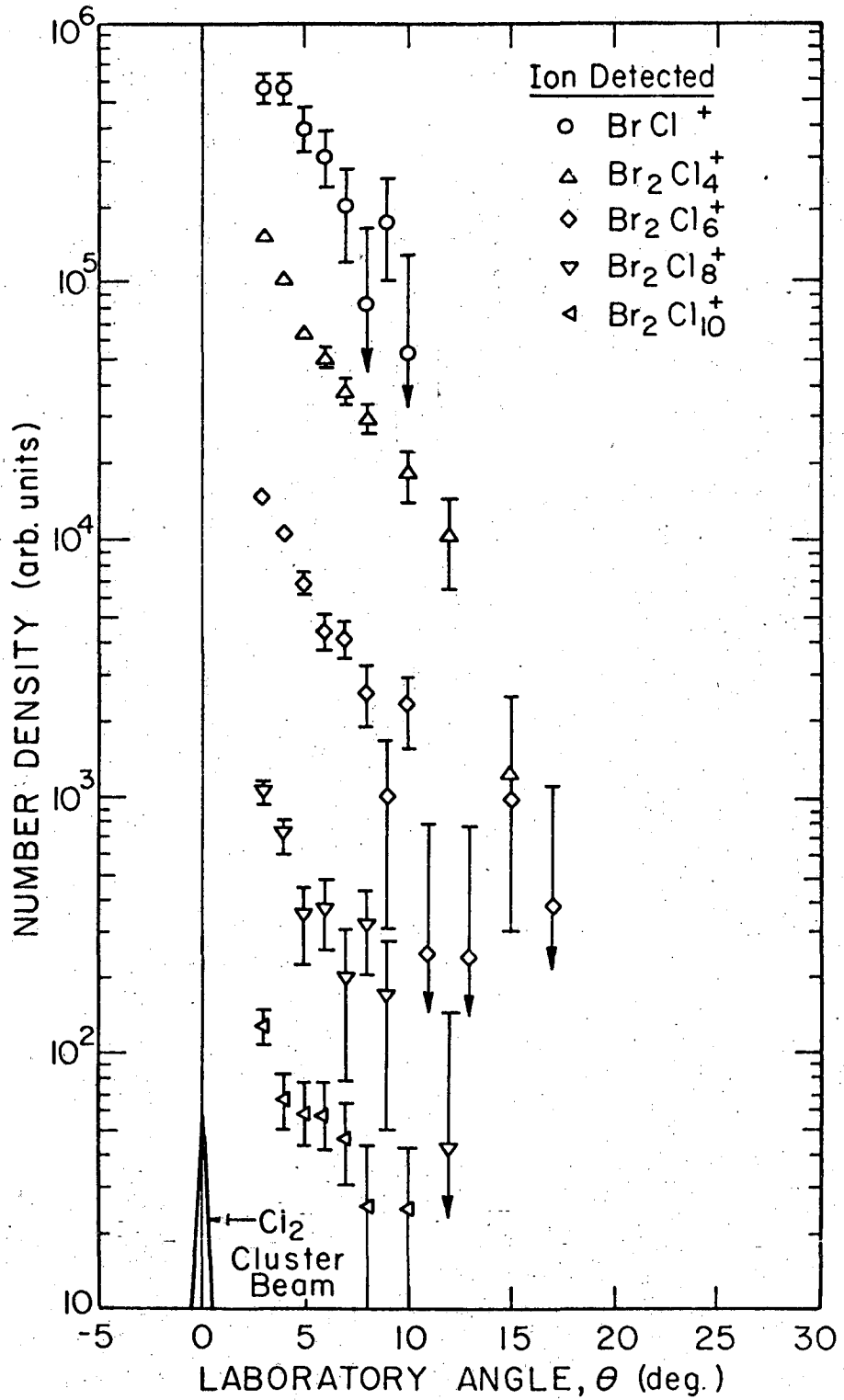

XBL756-6506

Fig. 7

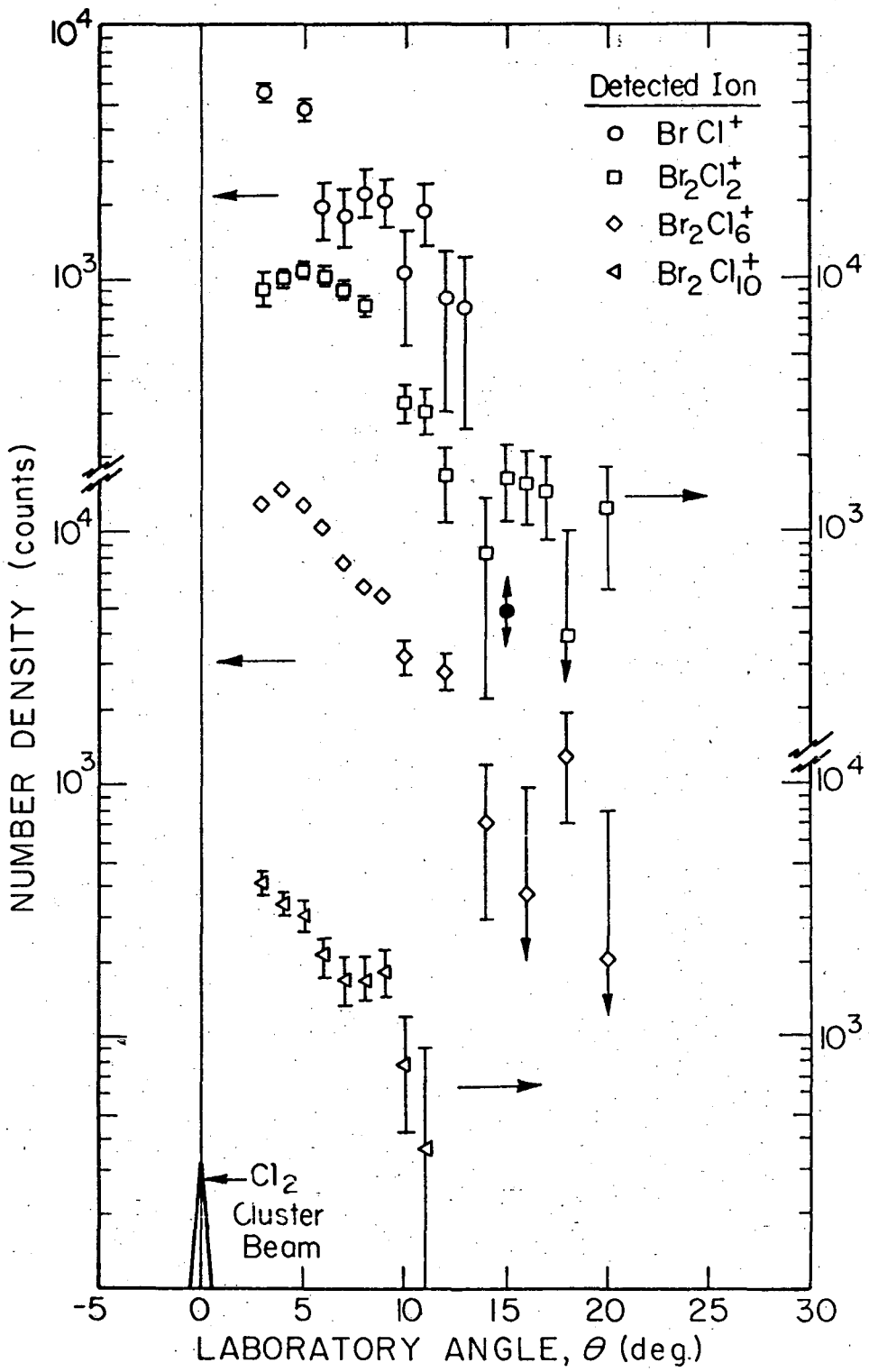

XBL 756-6507

Fig. 8

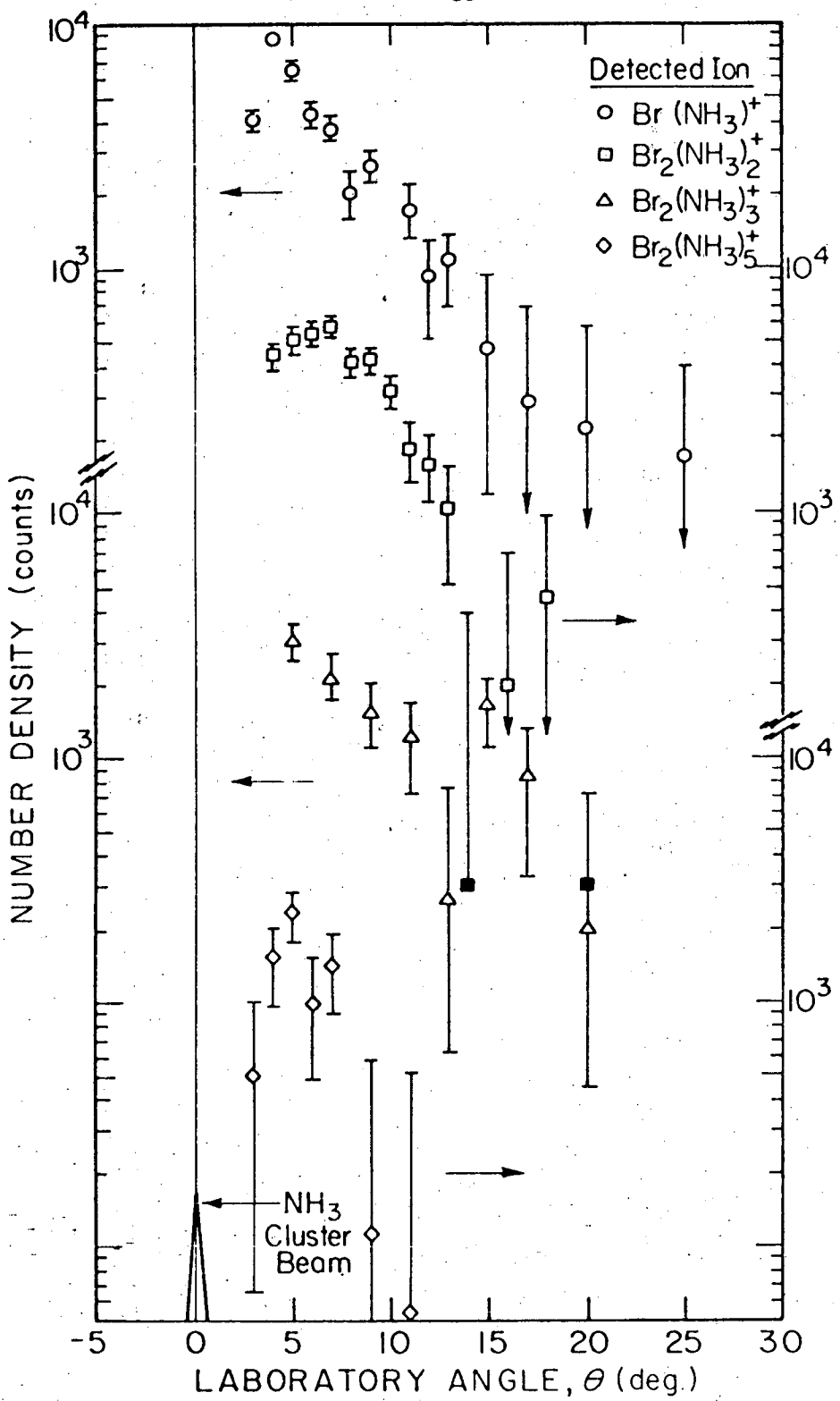

XBL 756-6508

Fig. 9

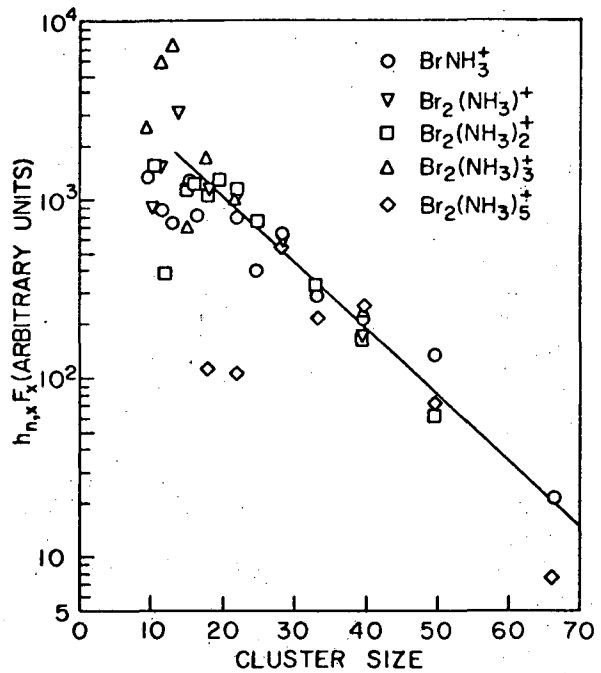
$BrNH_3^+$
$Br_2(NH_3)^+$
$Br_2(NH_3)_2^+$
$Br_2(NH_3)_3^+$
$Br_2(NH_3)_5^+$
$h_{n,x}F_x$ (ARBITRARY UNITS)
CLUSTER SIZE

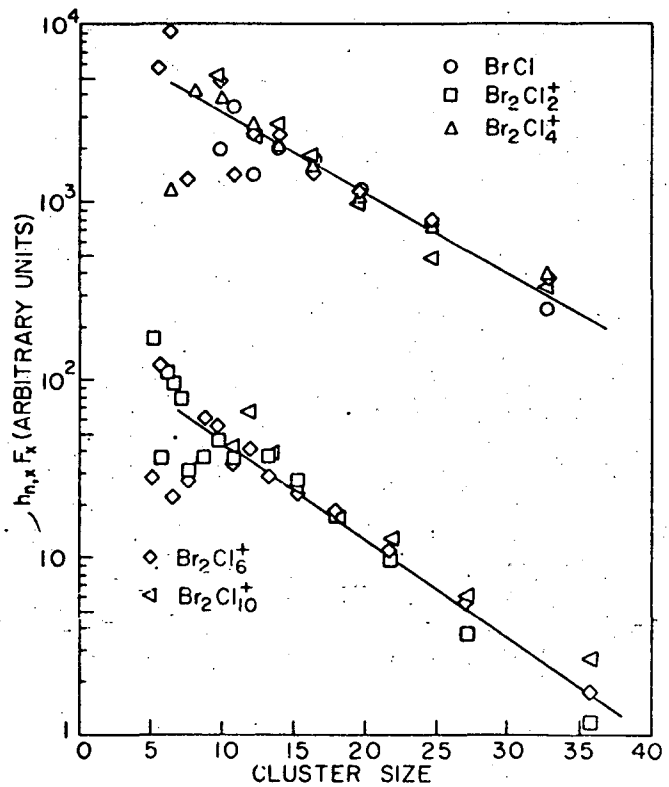
BrCl
$Br_2Cl_2^+$
$Br_2Cl_4^+$
$Br_2Cl_6^+$
$Br_2Cl_{10}^+$
$h_{n,x}F_x$ (ARBITRARY UNITS)
CLUSTER SIZE

Fig. 10

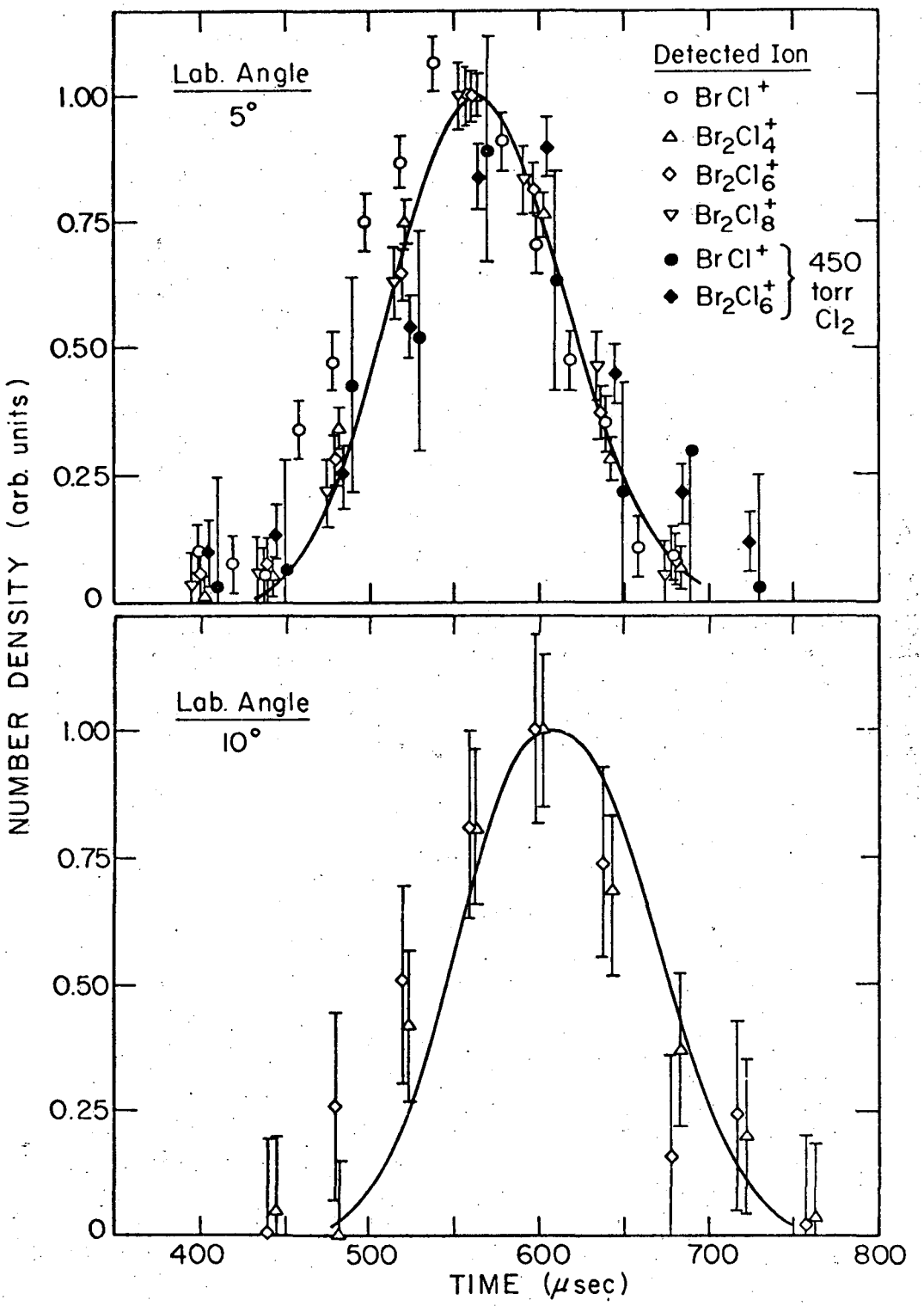

XBL756-6513

Fig. 11

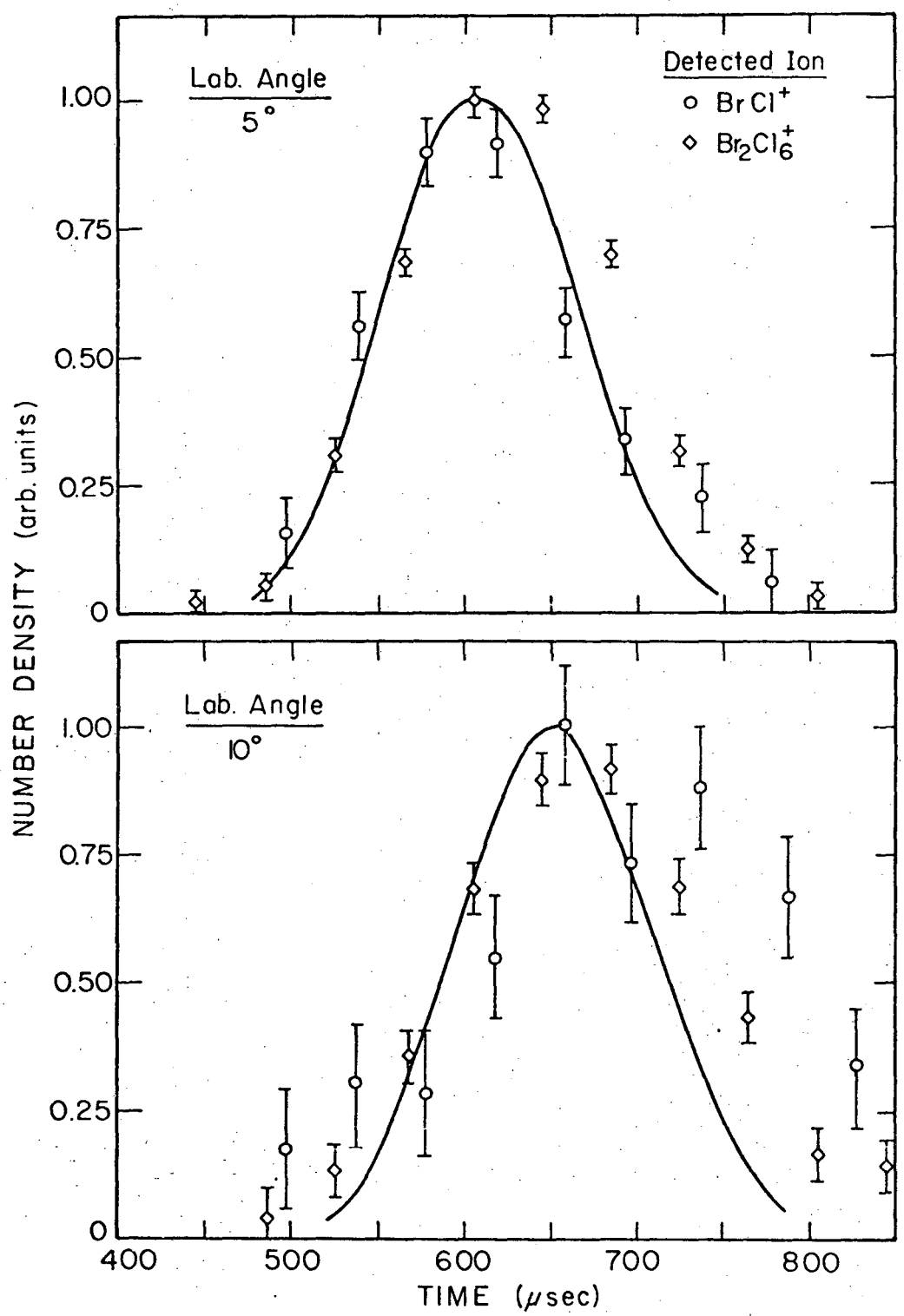

XBL 756-6514

Fig. 12

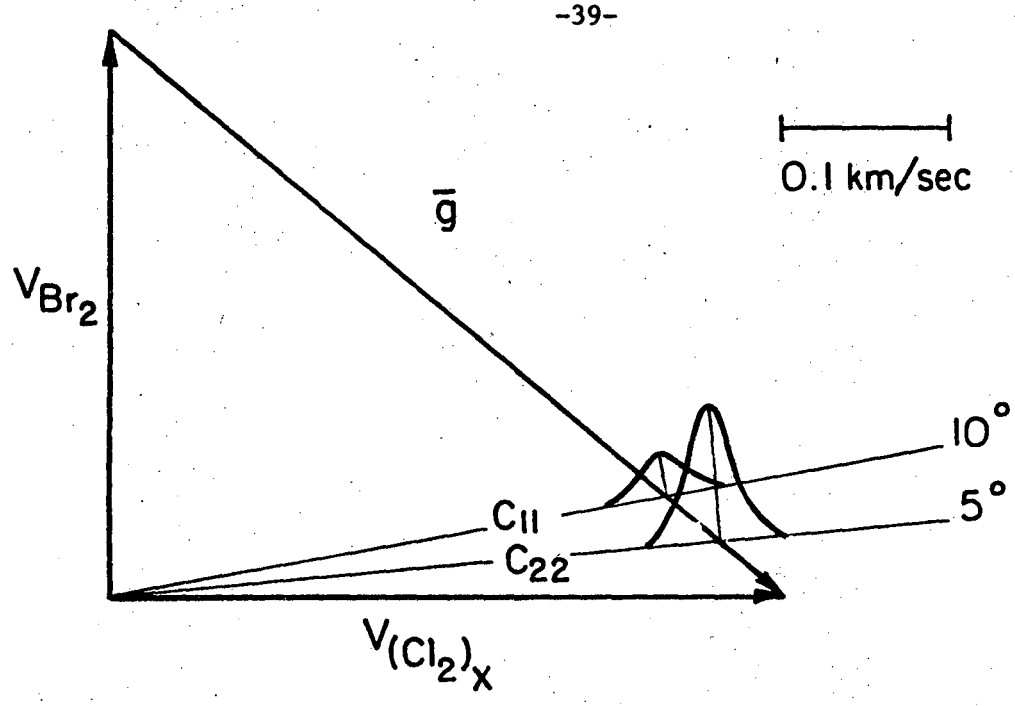

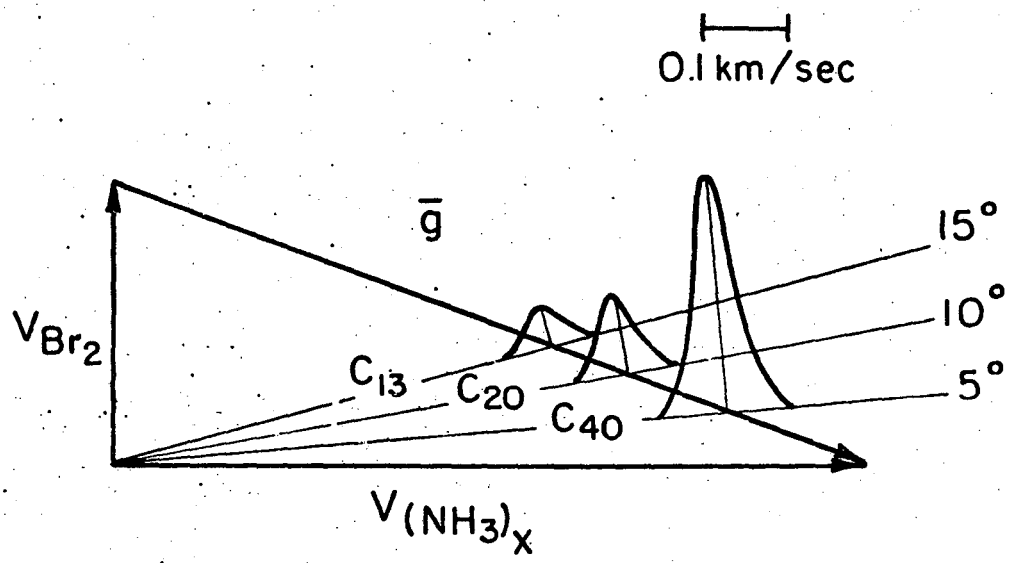

XBL 756-6623

Fig. 13

0 0 0 0 4 2 0 1 1 3 3

LEGAL NOTICE

This report was prepared as an account of work sponsored by the United States Government. Neither the United States nor the United States Energy Research and Development Administration, nor any of their employees, nor any of their contractors, subcontractors, or their employees, makes any warranty, express or implied, or assumes any legal liability or responsibility for the accuracy, completeness or usefulness of any information, apparatus, product or process disclosed, or represents that its use would not infringe privately owned rights.

TECHNICAL INFORMATION DIVISION
LAWRENCE BERKELEY LABORATORY
UNIVERSITY OF CALIFORNIA
BERKELEY, CALIFORNIA 94720